Int. J Heat Mass Transfer. Vol. 13, pp. 27–42. Pergamon Press 1970. Printed in Great Britain

COMPUTATIONAL AND EXPERIMENTAL STUDY OF THE EFFECT OF SECONDARY FLOW ON THE TEMPERATURE FIELD AND PRIMARY FLOW IN A HEATED HORIZONTAL TUBE

D. P. SIEGWARTH* and T. J. HANRATTY
Department of Chemistry and Chemical Engineering, University of Illinois, Urbana, Illinois

(*Received* 1 *May* 1969)

Abstract—The fully developed temperature field and axial velocity profile are measured for a fluid with a Prandtl number of 80 at the outlet of a long horizontal tube which is heated electrically. The defining partial differential equations are solved by finite difference techniques to obtain the secondary flow patterns as well as the temperature field and axial velocity field. Relatively large secondary flows are found for temperature differences between the wall and the fluid as low as 0·05°F. For $(GP)^{\frac{1}{4}}$ greater than 30 boundary layer theory appears to be a good approximation to the temperature field. There are large temperature gradients near the wall; the isotherms in the core are horizontal and there is a significant temperature variation in the vertical direction. Although the secondary flow had a large effect on the temperature field it had little effect on the axial velocity distribution as has been predicted for large Prandtl number. The secondary flow pattern shows relatively large upward velocities near the wall and small downward velocities in the core. The thicknesses of the velocity and temperature boundary layers are approximately equal. These results agree with a treatment of the problem, based on dimensional reasoning, that has been presented in a previous paper from this laboratory.

NOMENCLATURE

a, tube radius;
c, heat capacity;
G, Grashof number $= (a^3\beta g\rho^2\Delta T)/\mu^2$;
g, acceleration of gravity;
h, heat-transfer coefficient $= q/\Delta T$;
k, thermal conductivity of the fluid;
N, Nusselt number $= qa/\Delta Tk$;
P, pressure normalized with respect to $\rho\langle W\rangle^2$;
P, Prandtl number $= c\mu/k$;
q, rate of heat transfer to the fluid per unit area;
r, radial distance normalized with respect to a;
R, Reynolds number $= (a\langle W\rangle\rho)/\mu$;
P_z, $= \partial P/\partial z$;
T, temperature of the fluid;
T_W, temperature at the wall;
T_B, bulk averaged temperature of the fluid;
ΔT, $= T_W - T_B$;
t, $= (T - T_B)/(2qa/k)$;
u, velocity in the vertical direction normalized with respect to $\langle W\rangle$;
$\langle W\rangle$, bulk averaged velocity;
w, axial velocity normalized with respect to $\langle W\rangle$;
$\hat{w}$, $= w/P_z$;
x, distance in the vertical direction normalized with respect to a;
y, distance in the horizontal direction normalized with respect to a;
z, distance in axial direction normalized with respect to a;
β, coefficient of thermal expansion;
δ_T, normalization parameter for the thermal boundary layer;

* Presently with General Electric Co., San Jose, California.

θ, angle measured from the bottom of the tube;
μ, viscosity;
ξ, vorticity normalized with respect to $\langle W\rangle/a$;
ρ, density;
τ, time normalized with respect to $a/\langle W\rangle$;
ψ, stream function normalized with respect to $a\langle W\rangle$.

1. INTRODUCTION

AN ANALYSIS of the effect of the secondary flow arising from fluid density variations in a heated horizontal tube on the primary flow and on the temperature profile has been presented in a previous paper from this laboratory [1], to be referred to as SMRH. The analysis is supported by experiments and computer computations to be described in this paper. The system considered in SMRH is a long tube with a constant heat input per unit length and with a constant temperature around the inside circumference at any axial location. Far downstream, a fully developed condition is attained for which the velocity field is not changing in the direction of mean flow and for which the temperature of the fluid and the wall are increasing linearly with distance downstream. By studying these fully developed velocity and temperature profiles the difficulty of accounting for the previous history of the field is avoided.

This system has been approximated in the laboratory by electrically heating the outside of a 36-ft length of $2\frac{1}{2}$ in. i.d. pipe through which ethylene glycol is circulated. The pipe is insulated with 3 in. of glass wool to minimize heat losses to the surroundings. By using a relatively thick wall, 1 in., and a material of high thermal conductivity, aluminum, the heat flux to the outside was distributed in the pipe wall so that the temperature around the inside wall showed only a small variation even though the local heat-transfer coefficient changed by as much as 40-fold around the circumference. After establishing that a fully developed condition was attained the temperature profile and the velocity profile were measured at the outlet of the heat-transfer section.

A numerical solution of the partial differential equations describing the fully developed flow was obtained by finite difference techniques. These calculations had the advantage over the laboratory experiments in that they yielded direct information on the secondary flow. However, the stability of the calculational scheme limited the magnitude of the Grashof number which could be investigated. The laboratory study therefore complemented the numerical calculation both by providing a check on the numerical methods and by extending the range of variables.

The analysis presented in SMRH is based on the assumption of the existence of a thin thermal boundary layer near the wall and on the assumption that the isotherms outside the thermal boundary layer are horizontal. The validity of the boundary layer assumption depends on the magnitude of GP, since the thickness of the thermal boundary layer δ_T, is given as

$$\delta_T = a(GP)^{-\frac{1}{4}}, \tag{1}$$

where P is the Prandtl number, a is the tube radius and G is the Grashof number based on the radius of the tube and ΔT the difference between the wall temperature and bulk averaged temperature. It has also been shown that if $P = 1$ the axial velocity varies over the tube cross section in a manner similar to the temperature and that the change of the axial velocity and temperature in the core is of the same magnitude as the bulk averaged velocity $\langle W\rangle$ and the temperature difference ΔT. These conclusions for $P \cong 1$ are supported by the velocity and temperature measurements made with heated air by Mori *et al.* [2].

The experiments reported in this paper extend available experimental results to larger Prandtl numbers and lend support to some of the conclusions reached in SMRH regarding the effect of P. Conditions for these experiments have been

deliberately selected so that the effect of the density variation in the axial direction was small.

2. EXPERIMENTAL

The laboratory experiments were performed with a heat transfer section that is constructed of three 12 ft lengths. The inside diameter was bored to a diameter of 2·525 ± 0·005 in. and a microfinish of 20. Heat was supplied by $\frac{3}{16} \times$ 0·20 in. Chromel-A heating tape wound at a pitch of $\frac{3}{4}$ in. over two layers of insulating tape. An auxiliary heating tape was added to the exit end to compensate for axial heat conduction through the pipe wall. The fiberglass insulation that covered the whole length of the heat-transfer section limited the heat loss to the surroundings to about 1 per cent of the total power dissipated in the heaters.

The temperature of the wall was measured at intervals along the entire length of the pipe with thermocouples whose junctions were approximately $\frac{3}{32}$ in. from the inside wall. At the measuring station thermocouples were spaced at 45° intervals around the circumference of the pipe.

The temperature of the ethylene glycol fed to the heat-transfer section was carefully controlled. Therefore the bulk temperature T_B at any location in the heat-transfer section was calculated from the measured power supplied to the heating elements and heat losses through the insulation. (See equation 27 of SMRH.) Tests were conducted under conditions where $T_W - T_B$ was constant over the last 6 ft of the heat-transfer section.

Velocity and temperature profiles were measured 8 in. and 14 in. from the end of the heat-transfer section using a traversing mechanism that entered through the end of the pipe. The probe holder could pivot as well as rotate so that it was located at different radial positions to ±0·005 in. and at different angular positions to ±1·0°. The temperature probe consisted of a 30 gauge iron–constantan thermocouple cemented inside a $\frac{1}{8}$ in. piece of stainless steel tubing. A Pitot tube was used to measure the axial velocity gradient. The pressure difference was measured to ±0·005 mm Hg with a Pace Model P90D tranducer. The Pitot tube and pressure transducer were calibrated by making measurements under isothermal conditions for which the velocity profile in the pipe is known.

Details about the experimental procedures are to be found in a Ph.D. thesis by Siegwarth [3].

3. COMPUTER CALCULATIONS

The time dependent partial differential equations representing the vorticity, the stream function and the temperature were approximated by finite difference equations and solved on the computer. Initially the axial velocity profile was assumed to be parabolic. The steady state stream function calculated with this assumption was used to compute a new axial velocity distribution and the procedure was repeated.

In these calculations all velocities are normalized with respect to the bulk averaged velocity $\langle W \rangle$, lengths, with the radius a, pressures with respect to $\rho \langle W \rangle^2$. The average heat flow to the fluid per unit area q and the velocity $\langle W \rangle$ are not varying with time so the bulk average temperature T_B is constant. A dimensionless temperature t is defined as the difference between the fluid temperature T and the bulk averaged temperature normalized with respect to $2qa/k$ where k is the thermal conductivity of the fluid. A solution is sought for which the wall temperature T_W is not varying around the inside circumference of the pipe, but is varying with time. Therefore, although the average heat flux is constant the local heat flux varies with circumferential position and with time. If axial density gradients are neglected and the fully developed region of the heat transfer section is considered the dimensionless time dependent equations describing the vorticity, the stream function, the axial velocity and the temperature are as follows:

$$\xi_\tau + \frac{1}{r}(\psi_\theta \xi_r - \psi_r \xi_\theta) = \frac{1}{R}\nabla^2 \xi + \frac{2NG}{R^2}\left(t_r \sin\theta + \frac{1}{r} t_\theta \cos\theta\right) \quad (2)$$

$$\nabla^2 \psi = -\xi \quad (3)$$

$$w_\tau + \frac{1}{r}(\psi_\theta w_r - \psi_r w_\theta) = \frac{1}{R}\nabla^2 w - P_z \quad (4)$$

$$t_\tau + \frac{1}{r}(\psi_\theta t_r - \psi_r t_\theta) = \frac{1}{RP}\nabla^2 t - \frac{1}{RP} w. \quad (5)$$

In the above equations the Nusselt number N and the Reynolds number R are defined using the radius a and the temperature difference ΔT. Since T_W is a function of time, ΔT and N also vary with time. The boundary conditions are

$$\begin{aligned} &r = 1; \quad \psi = \psi_r = w = 0, \quad t = \frac{1}{2N} \\ &r = 0; \quad \psi, \xi, w, t \text{ are finite} \\ &\theta = 0; \quad \psi = \xi = w_\theta = t_\theta = 0 \\ &\theta = \pi; \quad \psi = \xi = w_\theta = t_\theta = 0. \end{aligned} \quad (6)$$

Another equation is needed to define the pressure gradient P_z. Since axial density gradients are neglected, the pressure gradient is constant over the cross section of the tube and (4) can be divided by P_z to give

$$\hat{w}_\tau + \frac{1}{r}(\psi_\theta \hat{w}_r - \psi_r \hat{w}_\theta) = \frac{1}{R}\nabla^2 \hat{w} - 1, \quad (7)$$

where

$$w = \hat{w} P_z. \quad (8)$$

Since the average velocity remains constant the following integral defines P_z:

$$P_z = \left[\pi / \int_0^\pi \int_0^1 \hat{w} r \, dr \, d\theta\right] \quad (9)$$

The values of ξ, ψ, w, t and P_z can be calculated for given values of R, P, and NG by solving (2), (3), (5), (7) and (9) using boundary conditions (6).

The vorticity and steam function were set equal to zero throughout the whole field at $\tau = 0$. Initially the temperature field is zero everywhere except at the wall and the heat flux is not varying around the circumference. From the definition of the dimensionless temperature $\partial t/\partial r = 0{\cdot}5$ at the wall for $\tau = 0$.

The numerical procedure was similar to that employed by Wilkes and Churchill [4] to solve the problem of free convection in a two-dimensional cavity where one side wall is heated and the other cooled. The vorticity and temperature equations were solved by an extension of the alternating direction implicit (A.D.I.) method [5, 6] and the stream function equation was solved using successive over relaxation.

The finite difference equations are written in cylindrical coordinates with variable mesh spacing in the radial direction. A fine radial grid spacing was used near the wall where the temperature and velocity gradients are large and a coarse spacing in the center where the gradients are small. Because of the singularity of the coefficients in the differential equations at the origin special attention had to be given to the formulation the difference equations at $r = 0$ [7]. Details of the numerical procedures are presented in a Ph.D. thesis by one of the authors [3].

Some of the differences from the work of Wilkes and Churchill are outlined in an appendix to this paper.

4. FULLY DEVELOPED TEMPERATURE PROFILES

Computed temperature distributions for $(GP)^{\frac{1}{4}} = 8{\cdot}33$ and for $(GP)^{\frac{1}{4}} = 31{\cdot}0$ are shown in Figs. 1 and 2. Measured temperature distributions for $(GP)^{\frac{1}{4}} = 31{\cdot}9$ and for $(GP)^{\frac{1}{4}} = 51{\cdot}3$ are shown in Figs. 3 and 4. In the absence of secondary flow the Nusselt number is 24/11. The computed $N = 4{\cdot}58$ for Fig. 1 indicates that even at small heating rates ($\Delta T \cong 0{\cdot}05°\text{F}$) free convection is having a strong effect on the heat transfer. For $(GP)^{\frac{1}{4}}$ greater than 30 boundary layer theory appears to be a good approximation to the temperature field. As previously found in experiments with air [2] the temperature in the core varies mainly in the vertical direction and

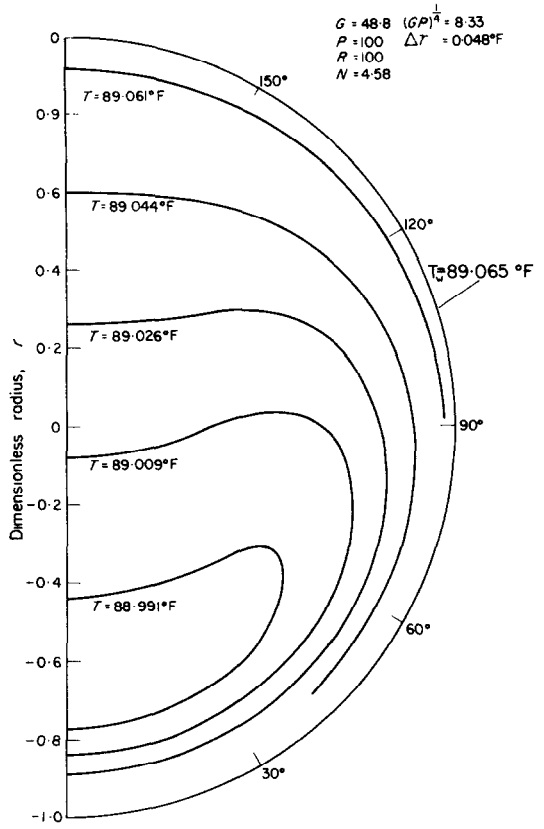

FIG. 1. Computed temperature distribution.

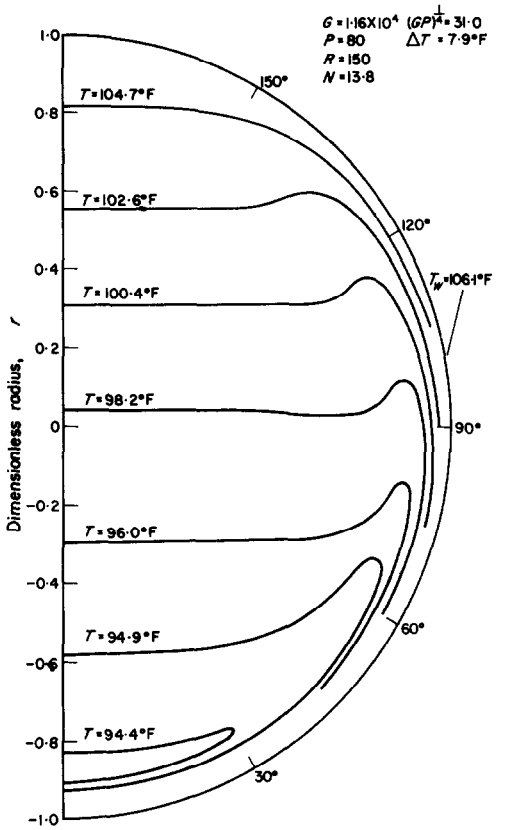

FIG. 2. Computed temperature distribution.

the magnitude of the variation is of the same order as ΔT.

The wall was not quite thick enough to maintain a uniform circumferential temperature at the inside. The wall temperature in Fig. 3 varies from 106·4°F at the bottom to 107·0°F at the top and in Fig. 4, from 150·5°F to 156·8°F. Considering this variation the agreement between the measurements in Fig. 3 and the computations in Fig. 4 are reasonable.

The variation of the local Nusselt number around the circumference for the results in Figs. 2 and 4 is shown in Fig. 5. It is seen that the local heat-transfer rate can vary considerably and that at the very top of the tube the heat-transfer rates are of the same magnitude as would be expected for laminar forced convection. The average of the Nusselt numbers in Fig. 5 is about 15 per cent higher than N. This reflects the errors in evaluating temperature gradients close to the wall.

Temperature profiles for different horizontal levels in the tube are presented in Figs. 6 and 7. The temperature boundary layer close to wall is clearly evident although its thickness is somewhat larger than is required for the asymptotic approximations in SMRH to be completely accurate.

5. AXIAL VELOCITY PROFILES

Although the secondary flow had a large effect on the temperature it had little effect on the axial velocity distribution. Measured and computed horizontal and vertical profiles shown in Figs. 8–11 are close to a parabolic shape, as

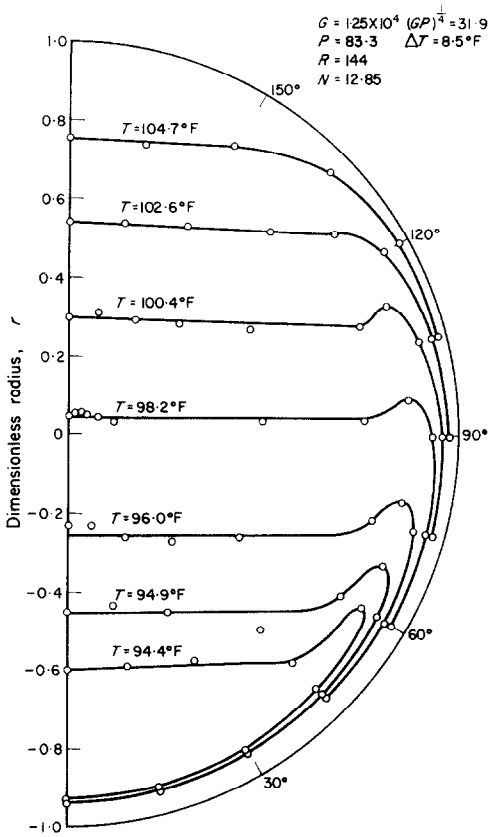

FIG. 3. Measured temperature distribution.

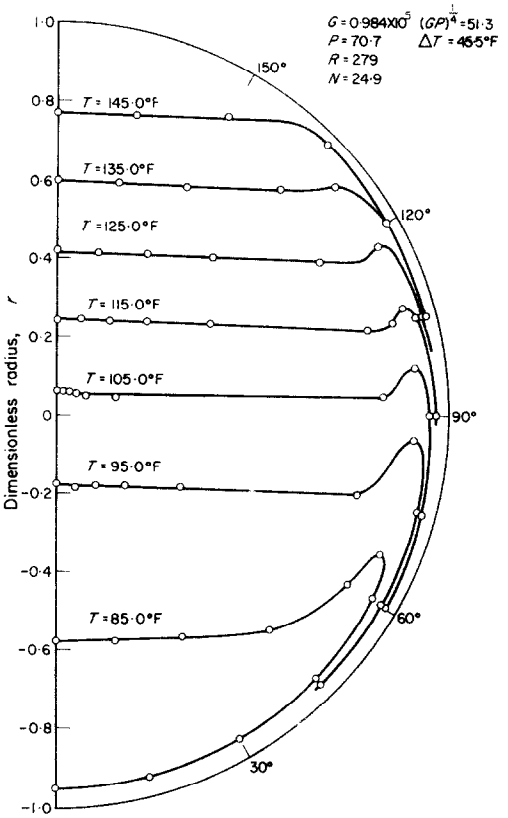

FIG. 4. Measured temperature distribution.

predicted in SMRH for large P. The slight differences in the computed profiles and a parabola indicate the Prandtl number was not quite large enough for secondary flow to be having a negligible effect on the axial velocity. The measurements in Figs. 10 and 11 show a small velocity increase in the bottom of the pipe due to secondary flow and symmetry about the vertical axis. However the maximum in the velocity profile appears to be above the horizontal axis. This trend is probably due to the decrease of viscosity with height in the pipe because of the increase in temperature. The change in temperature affected the viscous stresses in the fluid but it also affected the viscous correction applied to the readings from the Pitot tube. Some of the distortion could be due to errors in applying this viscous correction.

The difference from a parabolic shape cited above is less interesting than the similarity. It is therefore appropriate that we compare the results presented in this paper with the order of magnitude estimates in SMRH.

The estimated order of magnitude of the ratio of the inertia to the viscous terms in the equation describing the axial velocity distribution is $(PG)^{\frac{1}{2}}/P$. For the results shown in Figs. 8 and 10 this ratio is 0·39 and 0·60 respectively. It is apparent that it is not necessary for $(PG)^{\frac{1}{2}}/P$ to be exceedingly small for the secondary flow to be having an unimportant role.

In order for axial density gradients to have a

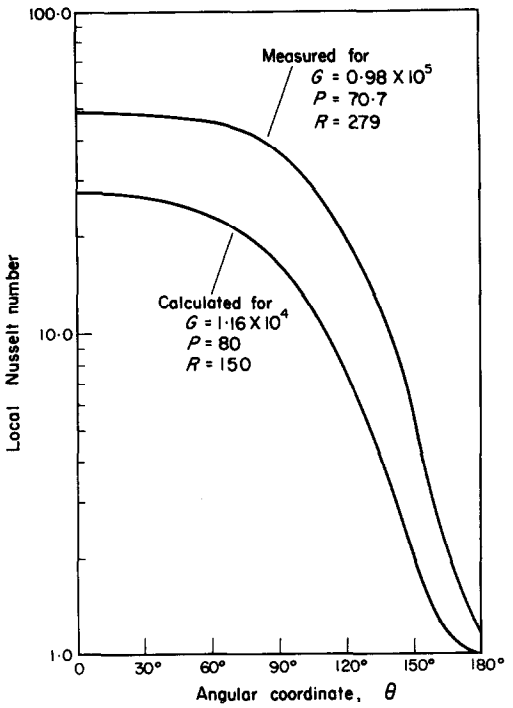

FIG. 5. Variation of the heat flux around the periphery.

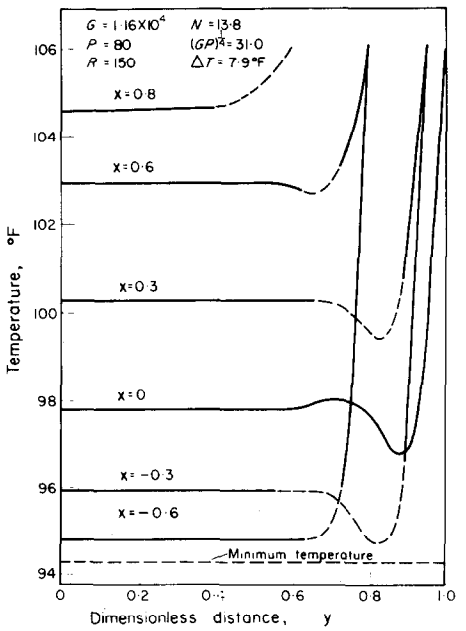

FIG. 6. Computed temperature profiles.

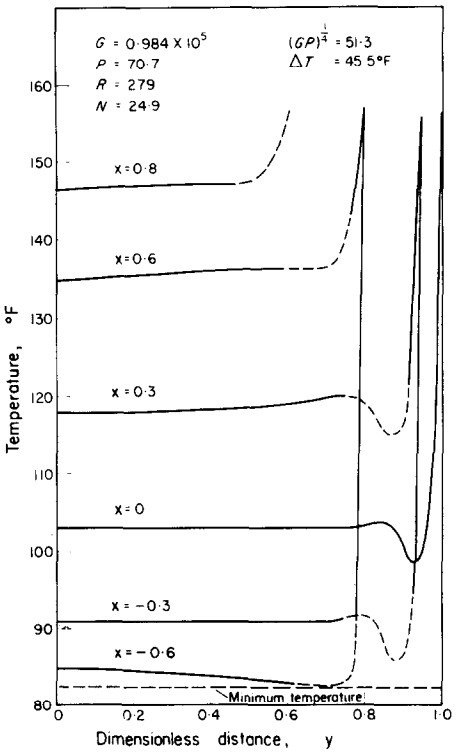

FIG. 7. Measured temperature profiles.

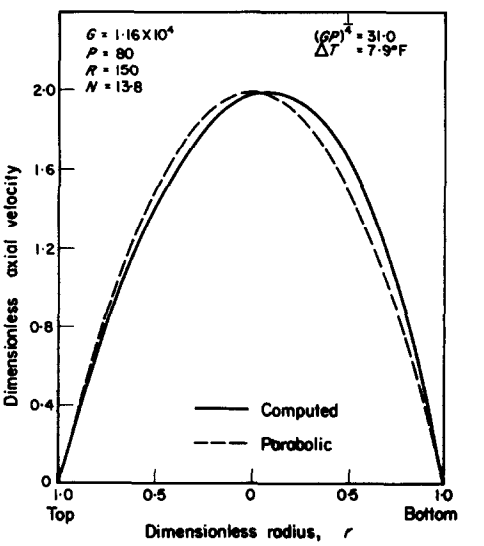

FIG. 8. Computed vertical velocity profile.

C

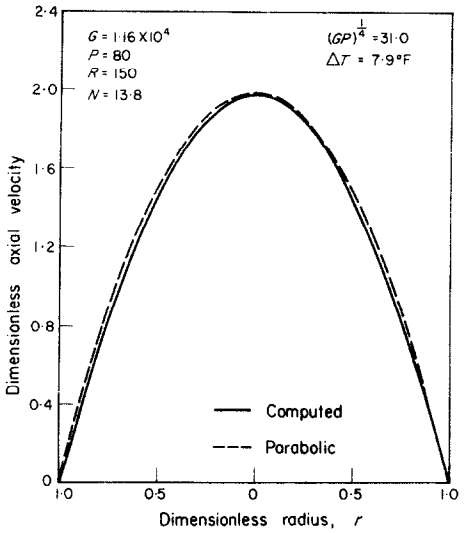

FIG. 9. Computed horizontal velocity profile.

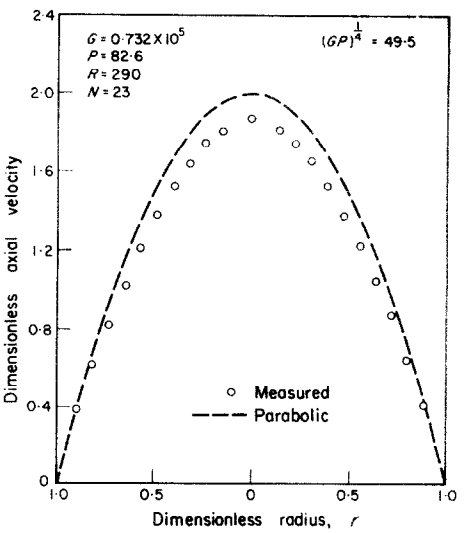

FIG. 11. Measured horizontal velocity profile.

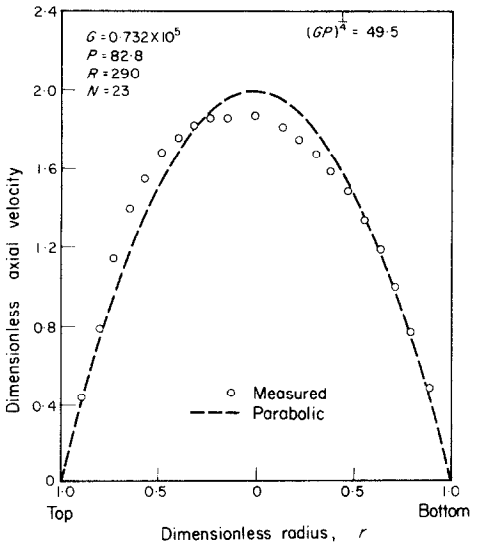

FIG. 10. Measured vertical velocity profile.

negligible effect it has been estimated in SMRH that $2NG/PR^2$ must be a small number. A more accurate assessment can be obtained for the experimental conditions treated in this paper by using the solution presented by del Casal and Gill [8] for the case of negligible effects due to secondary flow.

$$w = 2(1 - r^2) + \frac{1}{4}\frac{NG}{PR^2} r(1 - r^2)\cos\theta \quad (10)$$

It is seen that axial temperature gradients will have an effect on the velocity gradients at the wall of less than 10 per cent if NG/PR^2 is less than 0·8. For the results in Figs. 8 and 9 $NG/PR^2 = 0{\cdot}09$ and for Figs. 10 and 11 $NG/PR^2 = 0{\cdot}24$. It is apparent that axial density gradients have a negligible effect on the results presented in this paper.

6. SECONDARY FLOW PATTERNS

Calculated stream functions which have been made dimensionless with respect to the average axial velocity and the tube radius are shown in Figs. 12 and 13.

As the Grashof number increases the pattern becomes more asymmetric with respect to the horizontal and the gradient near the wall becomes large compared to the gradient in the center of the pipe. These trends are in agreement with the visual studies of R. D. Mikesell [9], who examined the motion of colored streamers in a heated horizontal pipe. The eye of the

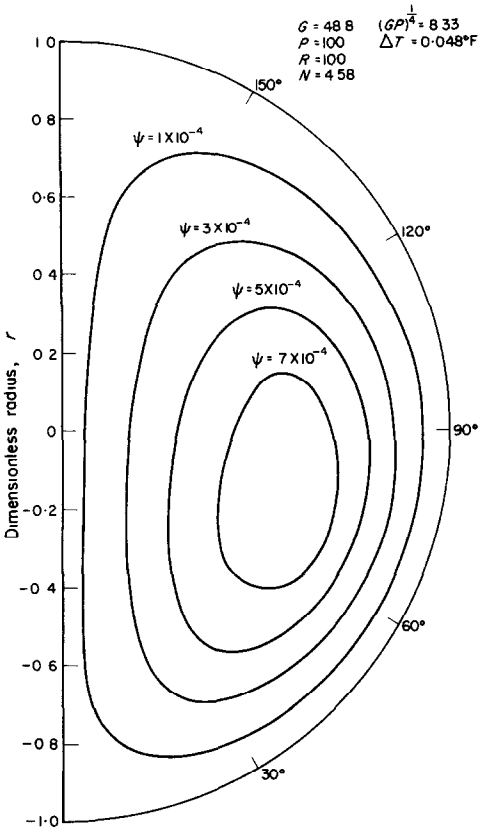

FIG. 12. Stream function for the secondary flow.

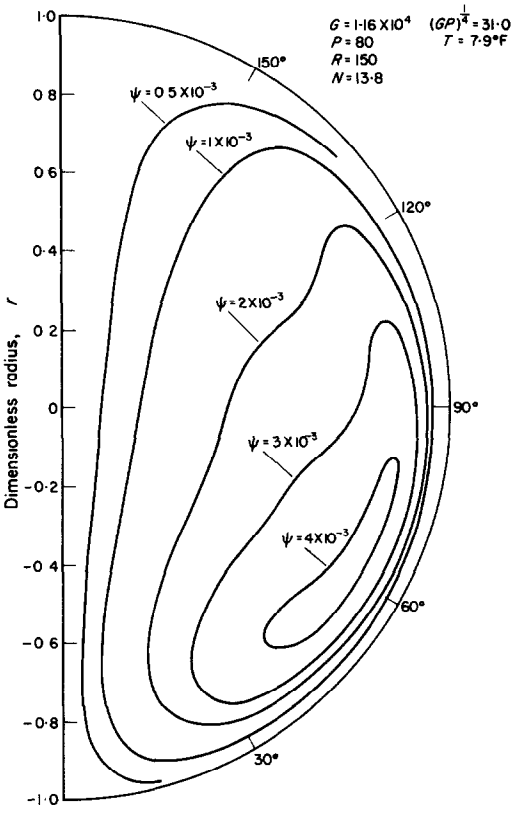

FIG. 13. Stream function for the secondary flow.

secondary pattern could easily be located by determining that place in the tube at which the colored streamer moved in a straight line. Mikesell found that the eye moved downward and closer to the wall as the Grashof number increased.

The vorticity distribution for $G = 1{\cdot}16 \times 10^4$ is shown in Fig. 14. The vorticity takes large negative values in the region of the wall, reaches its maximum positive value at $r = 0{\cdot}9$ and then decreases rapidly. The vorticity is quite small, that is of order 10^{-3}, in the center region where no lines of constant vorticity are shown. The vorticity profile for $\theta = 90°$ is shown in Fig. 15. Two types of secondary flow patterns were suggested in SMRH for $P \to \infty$, depending on whether the velocity of the return flow is small or large. As evidenced by the large temperature variation in the core, the results presented in this paper indicate a secondary flow pattern with a small return flow. This is more directly illustrated by the temperature and secondary velocity profiles shown in Figs. 16–18. Even for the relatively small value of $(GP)^{\frac{1}{4}} = 31$ a distinct boundary layer behavior is indicated. In order to indicate the extent of the thermal boundary layer the core temperatures, defined by horizontal isotherms, are extrapolated to the wall in Figs. 16–18. As suggested in SMRH the temperature and velocity boundary layers have approximately the same thicknesses.

It is predicted in SMRH that a consequence of the horizontal isotherms and the neglection of thermal conduction in the core is that the

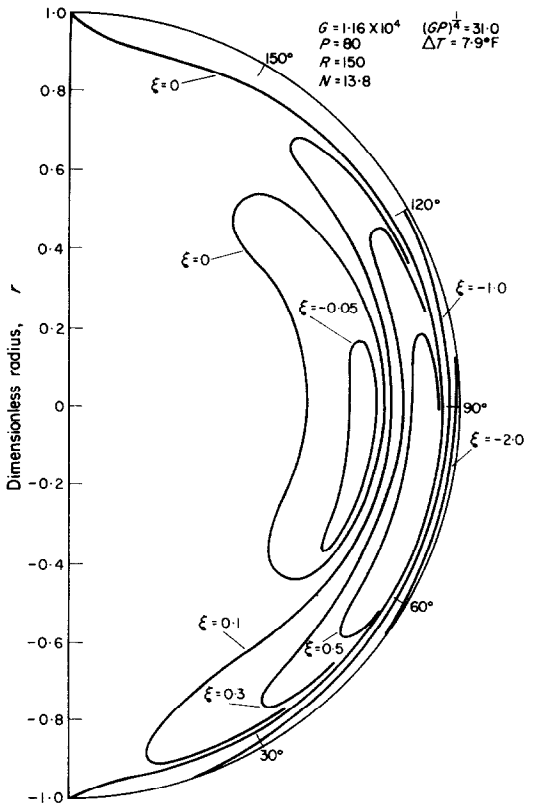

FIG. 14. Vorticity distribution.

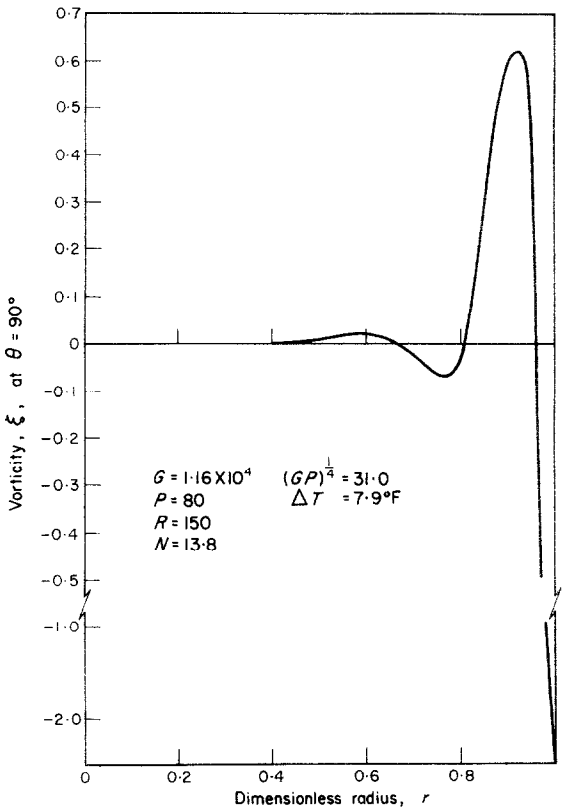

FIG. 15. Vorticity profile at $\theta = 90°$.

ratio of the vertical velocity component to the axial velocity component should be a constant on any horizontal level in the core. Table 1 indicates that this prediction is confirmed for the calculated velocity field for $G = 1{\cdot}16 \times 10^4$. In the Table x and y are dimensionless distances in the vertical and horizontal directions.

ACKNOWLEDGEMENTS

We are grateful to Dr. R. A. Schmitz for help in formulating the finite difference equations. We also acknowledge support received from the National Science Foundation.

REFERENCES

1. D. P. SIEGWARTH, R. D. MIKESELL, T. C. READAL and T. J. HANRATTY, To be published in *Int. J. Heat Mass Transfer*.
2. Y. MORI, K. FUTAGAMI, S. TOKUDU and M. NAKAMURA, Forced convective heat transfer in uniformly heated horizontal tubes, *Int. J. Heat Mass Transfer* **9**, 453 (1966).
3. D. P. SIEGWARTH, Effect of free convection on laminar flow through a horizontal pipe, Ph.D. thesis, University of Illinois, Urbana (1968).
4. J. O. WILKES and S. W. CHURCHILL, The finite-difference computation of natural convection in a rectangular enclosure, *A.I.Ch.E. Jl.* **12**, 161 (1966).
5. D. W. PEACEMAN and H. H. RACHFORD, The numerical solution of parabolic and elliptic differential equations, *J. Soc. Indust. Appl. Math.* **3**, 22 (1955).
6. J. DOUGLAS, On the integration of $(\partial^2 u/\partial x^2) + (\partial^2 u/\partial t) = (\partial \mu/\partial t)$ by implicit methods, *J. Soc. Indust. Appl. Math.* **3**, 42 (1955).
7. E. L. ALBASINY, On the numerical solution of a cylindrical heat-conduction problem, *Q. Jl Mech. Appl. Math.* **13**, 374 (1960).
8. E. DEL CASAL and W. GILL, A note on natural convection effects in fully developed horizontal tube flow, *A.I.Ch.E. Jl* **8**, 570 (1962).
9. R. D. MIKESELL, The effect of heat transfer on the flow in a horizontal pipe, Ph.D. thesis, University of Illinois, Urbana (1963).
10. C. E. PEARSON, On computational method for viscous flow problems, *J. Fluid Mech.* **21**, 611 (1965).

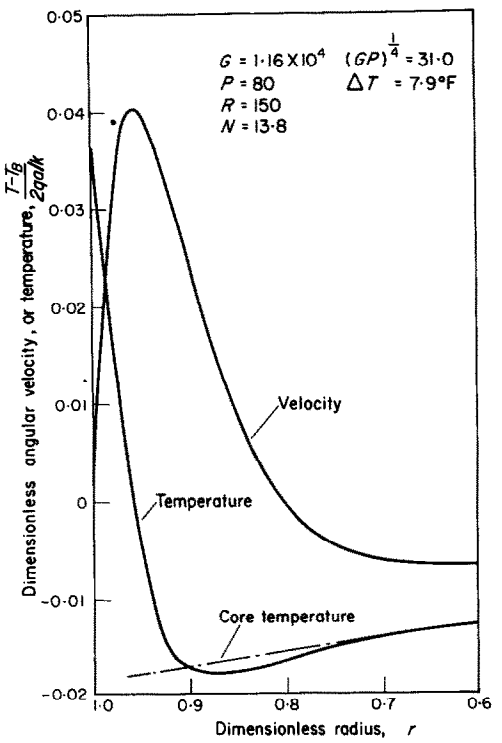

FIG. 16. Temperature and velocity distributions in the boundary layer for $\theta = 45°$.

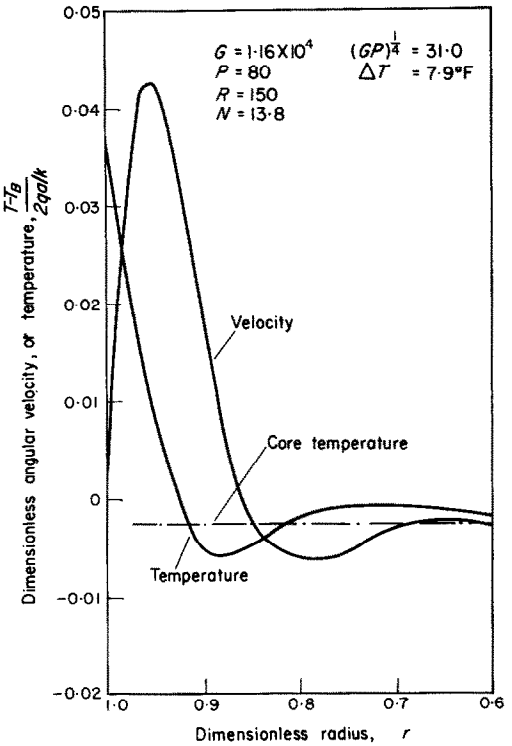

FIG. 17. Temperature and velocity distributions in the boundary layer for $\theta = 90°$.

APPENDIX

A. The Use of a Spacing with Variable Mesh Size

A section of the finite-difference network is shown in Fig. 19. The approximations of the angular derivatives are obtained by using standard centered difference formulas.

$$\frac{\partial u}{\partial \theta} = \frac{u_{j+1} - u_{j-1}}{2\Delta\theta} \tag{A.1}$$

$$\frac{\partial^2 u}{\partial \theta^2} = \frac{u_{j+1} - 2u_j + u_{j-1}}{\Delta\theta^2}. \tag{A.2}$$

The finite-difference representations of radial derivatives are more complicated because Δr_1 in Fig. 19 may not equal Δr_2. By using a linear interpolation the first derivative with respect to r at the radial position i can be written as follows:

$$\left.\frac{\partial u}{\partial r}\right|_i = \left[\left.\frac{\partial u}{\partial r}\right|_{i+1} - \left.\frac{\partial u}{\partial r}\right|_{i-1}\right]\frac{\Delta r_1}{\Delta r_1 + \Delta r_2} + \left.\frac{\partial u}{\partial r}\right|_{i-1}. \tag{A.3}$$

The derivatives at $i - 1$ and $i + 1$ are approximated by forward and backward differences to give

$$\left.\frac{\partial u}{\partial r}\right|_{i-1} = \frac{u_i - u_{i-1}}{\Delta r_1} \tag{A.4}$$

$$\left.\frac{\partial u}{\partial r}\right|_{i+1} = \frac{u_{i+1} - u_i}{\Delta r_2} \tag{A.5}$$

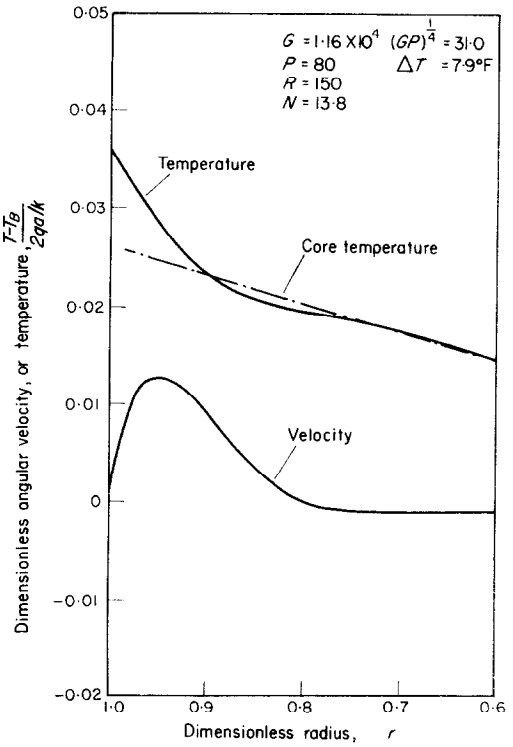

FIG. 18. Temperature and velocity distributions in the boundary layer for $\theta = 135°$.

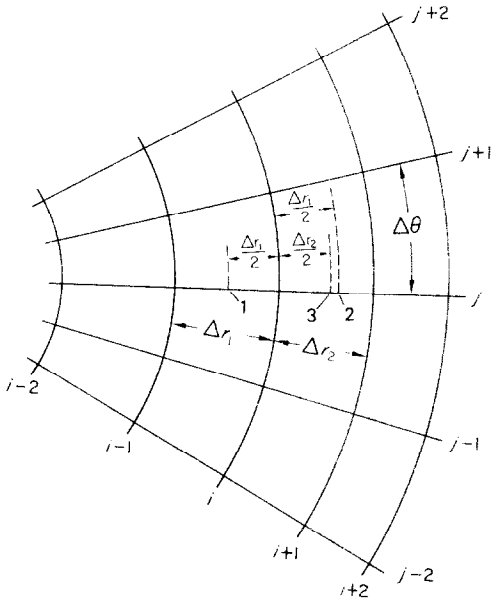

FIG. 19. Finite-difference network.

The following relation for the first derivative is obtained by substituting (A.4) and (A.5) into (A.3)

$$\left.\frac{\partial u}{\partial r}\right|_i = f_1 u_{i+1} + (f_2 - f_1)\, u_i - f_2 u_{i-1}, \quad \text{(A.6)}$$

where

$$f_1 = \frac{1}{\Delta r_2}\left(\frac{\Delta r_1}{\Delta r_1 + \Delta r_2}\right) \quad \text{(A.7)}$$

$$f_2 = \frac{1}{\Delta r_1}\left(\frac{\Delta r_1}{\Delta r_1 + \Delta r_2}\right). \quad \text{(A.8)}$$

If the radial positions 1, 2 and 3 are defined as shown in Fig. 19, the second derivative with respect to r can be written as

Table 1. Ratio of u/w in the core

y	$x = -0{\cdot}6$	$x = -0{\cdot}3$	$x = 0$	$x = 0{\cdot}3$	$x = 0{\cdot}6$
0	−0·00637	−0·00344	−0·00249	−0·00216	−0·00221
0·08	—	−0·00340	—	−0·00213	—
0·1	—	—	−0·00249	—	—
0·16	−0·00628	—	—	—	−0·00219
0·17	—	−0·00339	—	−0·00215	—
0·2	—	—	−0·00250	—	—
0·3	—	−0·00340	−0·00251	−0·00217	—
0·35	−0·00564	—	—	—	−0·00229
0·4	—	—	−0·00255	—	—
0·5	—	—	−0·00263	—	—
0·52	—	−0·00344	—	−0·00203	—
0·6	—	—	−0·00213	—	—
0·7	—	—	−0·00279	—	—

$$\left.\frac{\partial^2 u}{\partial r^2}\right|_i = \frac{(\partial u/\partial r)|_2 - (\partial u/\partial r)|_1}{\Delta r_1} \quad \text{(A.9)}$$

By linear interpolation the first derivative at point 2 is given by

$$\left.\frac{\partial u}{\partial r}\right|_2 = \left[\left.\frac{\partial u}{\partial r}\right|_3 - \left.\frac{\partial u}{\partial r}\right|_1\right]\left(\frac{2\Delta r_1}{\Delta r_1 + \Delta r_2}\right) + \left.\frac{\partial u}{\partial r}\right|_1 \quad \text{(A.10)}$$

The approximations of the first derivative at the points 1 and 3 are

$$\left.\frac{\partial u}{\partial r}\right|_1 = \frac{u_i - u_{i-1}}{\Delta r_1} \quad \text{(A.11)}$$

$$\left.\frac{\partial u}{\partial r}\right|_3 = \frac{u_{i+1} - u_i}{\Delta r_2} \quad \text{(A.12)}$$

The expression for the second derivative is obtained by substituting (A.10), (A.11) and (A.12) into (A.9).

$$\left.\frac{\partial^2 u}{\partial r^2}\right|_i = g_1 u_{i+1} - (g_1 + g_2) u_i + g_2 u_{i-1} \quad \text{(A13)}$$

$$g_1 = \frac{1}{\Delta r_2}\left(\frac{2}{\Delta r_2 + \Delta r_1}\right) \quad \text{(A.14)}$$

$$g_2 = \frac{1}{\Delta r_1}\left(\frac{2}{\Delta r_2 + \Delta r_1}\right). \quad \text{(A.15)}$$

B. Evaluation of the Stream Function

The stream function at time $(n + 1)\Delta\tau$ is computed by the method of successive over relaxation. If $\psi_{i,j}^{(m)}$ denotes the mth approximation of the stream function at time $(n + 1)\Delta\tau$, the next approximation is calculated as

$$\psi_{i,j}^{(m+1)} = (1 - \Omega)\psi_{i,j}^{(m)} + \frac{\Omega}{Q}\left[\xi_{i,j,n+1} + \left(g_1 + \frac{f_1}{r_i}\right)\psi_{i+1,j}^{(m)} + \left(g_2 - \frac{f_2}{r_i}\right)\psi_{i-1,j}^{(m+1)} + \frac{1}{r_i^2\,\Delta\theta^2}\left(\psi_{i,j+1}^{(m)} + \psi_{i,j-1}^{(m+1)}\right)\right], \quad \text{(A.16)}$$

where

$$Q = g_1 + g_2 - \frac{1}{r_i}(f_2 - f_1) + \frac{2}{r_i^2\,\Delta\theta^2}. \quad \text{(A.17)}$$

If (A.16) is solved at each mesh point for progressively increasing values of i and j, all quantities on the right-hand side are known. The stream function at the new time is obtained by iterating (A.16) until the difference between the $\psi_{i,j}$ calculated from two successive iterations is less than some predetermined parameter. The criterion used in this work is

$$\psi_{i,j}^{(m+1)} - \psi_{i,j}^{(m)} < 0{\cdot}001\,\psi_{i,j}^{(m+1)}. \quad \text{(A.18)}$$

It was found experimentally that if $\Omega = 1{\cdot}5$ only one iteration was needed, except at very small times. Therefore a constant value of $\Omega = 1{\cdot}5$ was used for the relaxation parameter.

C. Values of the Variables on the Boundaries

The local Nusselt number is calculated from the temperature gradient at the wall after each time step.

$$N_{j,n+1} = \frac{(\partial t/\partial r)|_{I,j,n+1}}{t_{I,n+1}}. \quad \text{(A.19)}$$

Let the mesh point next to the boundary be designated by r_{I-1} and that at the second mesh point away be r_{I-2}. Define Δr_1 and Δr_2 as follows:

$$\Delta r_1 = 1 - r_{I-1} \quad \text{(A.20)}$$

$$\Delta r_2 = r_{I-1} - r_{I-2}. \quad \text{(A.21)}$$

The backward finite-difference approximation, correct to the order of Δr_1^2, for the temperature gradient at the wall is

$$\left.\frac{\partial t}{\partial r}\right|_{I,j,n} = \frac{3t_{I,j,n} - 4t_{I-1,j,n} + t_{k,j,n}}{2\Delta r_1} \quad \text{(A.22)}$$

The temperature at point r_k is calculated by linear interpolation.

$$t_{k,j,n} = t_{I-1} + \frac{\Delta r_1}{\Delta r_2}(t_{I-2} - t_{I-1}). \quad \text{(A.23)}$$

Since t_I for time step $n+1$ is calculated from the average of the Nusselt number around the circumference at the end of time step n,

$$t_{I,n+1} = \frac{1}{2N_n} \tag{A.24}$$

If (A.22), (A.23) and (A.24) are substituted into (A.19),

$$N_{j,n+1} = 2N_n\left[\frac{1{\cdot}5}{\Delta r_1}t_{I,j,n} - \left(\frac{3\Delta r_2 + \Delta r_1}{2\Delta r_1 + 2\Delta r_2}\right)t_{I-1,j,n} + \frac{0{\cdot}5}{\Delta r_2}t_{I-2,j,n}\right] \tag{A.25}$$

The new value of the average Nusselt number at time $(n+1)\Delta\tau$, taken as

$$N_{n+1} = SN_n + (1-S)\frac{2}{\pi}\int_0^{\theta} N_{j,n+1}\,\mathrm{d}\theta, \tag{A.26}$$

is used to evaluate the wall temperature for the next time step. It was found that this boundary condition causes instabilities near the boundary when $S = 0$. A value of $S = 0{\cdot}8$ was used in the calculations.

The vorticity at the boundary also varies with time. Wilkes and Churchill [4] computed new wall vorticites by using a Taylor series expansion for the stream function in the vicinity of the wall. This procedure has been modified by using the smoothing factor suggested by Pearson [9]. Both ψ and $\partial\psi/\partial r$ are zero at the wall. The Taylor series expansion for ψ can therefore be written as follows:

$$\psi_{I-1,J} = \frac{\Delta r_1^2}{2!}\frac{\partial^2\psi}{\partial r^2}\bigg|_{r=1} - \frac{\Delta r_1^3}{3!}\frac{\partial^3\psi}{\partial r^3}\bigg|_{r=1} \tag{A.27}$$

$$\psi_{I-2,J} = \frac{(\Delta r_1 + \Delta r_2)^2}{2!}\frac{\partial^2\psi}{\partial r^2}\bigg|_{r=1} - \frac{(\Delta r_1 + \Delta r_2)^3}{3!}\frac{\partial^3\psi}{\partial r^3}\bigg|_{r=1} \tag{A.28}$$

If

$$\frac{\partial^3\psi}{\partial r^3}\bigg|_{r=1}$$

is eliminated between (A.27) and (A.28)

$$\frac{\partial^2\psi}{\partial r^2}\bigg|_{r=1} = 2\left[\left(\frac{\Delta r_1 + \Delta r_2}{\Delta r_1^3}\right)\psi_{I-1,J} - \frac{1}{(\Delta r_1 + \Delta r_2)^2}\psi_{I-2,J}\right] \tag{A.29}$$

where Δr_1 and Δr_2 are given by (A.20) and (A.21). On the boundary $\xi = -\partial^2\psi/\partial r^2$, so

$$\xi_{I,j,n+1} = S\xi_{I,J,n} - 2(1-S)\left[\left(\frac{\Delta r_1 + \Delta r_2}{\Delta r_1^3}\right)\psi_{I-1,J,n} - \frac{1}{(\Delta r_1 + \Delta r_2)^2}\psi_{I-2,J,n}\right] \tag{A.30}$$

Two different values of the smoothing factor were used. For $G = 49$, $S = 0$ and for $G = 1{\cdot}16 \times 10^4$, $S = 0{\cdot}8$.

At the point $r = 0$ $(i = 0)$ the stream function and vorticity are zero. The temperature and axial velocity are calculated from (4) and (5). Terms in these differential equations whose coefficients go to infinity as $r \to 0$ are evaluated by considering the limit as suggested by Albasiny [7]. The temperature equation which applies at $r = 0$ is

$$\frac{\partial t}{\partial\tau} + \frac{\partial^2\psi}{\partial\theta\partial r}\frac{\partial t}{\partial r} - \frac{\partial\psi}{\partial r}\frac{\partial^2 t}{\partial\theta\partial r} = \frac{1}{RP}\left(2\frac{\partial^2 t}{\partial r^2} + \frac{1}{2}\frac{\partial^4 t}{\partial\theta^2\partial r^2} - w\right) \tag{A.31}$$

Equation (A.31) can be used to calculate the temperature at $r = 0$ on the ray $\theta = \lambda/2$ $(j = l)$ where due to symmetry, $t_{1,l,n} = t_{-1,l,n}$, $t_{1,l+1,n} = t_{-1,l-1,n}$, $t_{1,l-1,n} = t_{-1,l+1,n}$ and $\psi_{1,l,n} = -\psi_{-1,l,n}$. If these symmetry conditions are used in the finite difference approximation of (A.31), the following equation is obtained for the first half time step:

$$\frac{\bar{t}_{0,l} - t_{0,l,n}}{\Delta\tau/2} - \frac{\psi_{1,l,n}}{\Delta r}\left(\frac{t_{1,l+1,n} - t_{1,l-1,n}}{2\Delta r\,\Delta\theta}\right)$$

$$= \frac{2}{RP}\left[\frac{2(\bar{t}_{1,l} - \bar{t}_{0,l})}{\Delta r^2} + \frac{1}{2}\left(\frac{t_{1,l+1,n} - 2t_{1,l,n} + t_{1,l-1,n}}{\Delta r^2\,\Delta\theta^2}\right)\right] - \frac{1}{RP} w_{0,l,n} \quad \text{(A.32)}$$

For the second half of the time step

$$\frac{t_{0,l,n+1} - \bar{t}_{0,l}}{\Delta\tau/2} - \frac{\psi_{1,l,n}}{\Delta r}\left(\frac{t_{1,l+1,n} - t_{1,l-1,n}}{2\Delta r\,\Delta\theta}\right) = \frac{2}{RP}\left[\frac{2(\bar{t}_{1,l} - t_{0,l})}{\Delta r^2} + \frac{1}{2}\left(\frac{t_{1,l+1,n} - 2t_{1,l,n} + t_{1,l-1,n}}{\Delta r^2\,\Delta\theta^2}\right)\right] - \frac{1}{RP} w_{0,l,n} \quad \text{(A.33)}$$

Equation (A.32) is implicit in r so it is necessary to invert a matrix for the ray $\theta = \lambda/2$ in order to calculate $\bar{t}_{0,l}$. Equation (A.33) is explicit so $t_{0,l,n+1}$ can be calculated directly from it.

The values of the unknowns are much more easily obtained on the boundaries $\theta = 0$ and $\theta = \pi$ than at the wall or at $r = 0$. The vorticity and stream function are zero there. The axial velocity and temperature are obtained by using the symmetry conditions. For example at $\theta = 0$

$$\hat{w}_{i,1} = \hat{w}_{i,-1} \quad \text{(A.34)}$$

$$t_{i,1} = t_{i,-1} \quad \text{(A.35)}$$

$$\psi_{i,1} = -\psi_{i,-1}. \quad \text{(A.36)}$$

Equations for the temperature and axial velocity on $\theta = 0$ are obtained by substituting (A.34), (A.35) and (A.36) into the finite difference representations of (5) and (7).

D. Procedure

The computational procedure to go from $n\Delta\tau$ to $(n + 1)\Delta\tau$ is as follows:

(1) Solve for the temperature at the new time $(n + 1)\Delta\tau$. The finite difference representation of (5) is used for the interior points. Equations (A.24), (A.32), (A.33), and (A.35) are used to define the temperature on the boundaries.

(2) Equation (A.30) is used to evaluate the vorticity at the solid boundary.

(3) The finite difference representation of (2) is used to calculate ξ_{n+1}.

(4) Equation (A.16) is solved for ψ_{n+1}.

(5) Check the vorticity to see if it has converged. If not return to (1).

ETUDE EXPÉRIMENTALE ET NUMÉRIQUE DE L'EFFET DE L'ÉCOULEMENT SECONDAIRE SUR LE CHAMP DE TEMPÉRATURE ET L'ÉCOULEMENT PRIMAIRE DANS UN TUBE HORIZONTAL CHAUFFÉ.

Résumé—Le champ de température et le profil de vitesse axiale entièrement développé sont mesurés pour un fluide avec un nombre de Prandtl de 80 à la sortie d'un long tube horizontal qui est chauffé électriquement. Les équations aux dérivées partielles de définition sont résolues par des techniques de différences finies pour obtenir les configurations d'écoulement secondaire ainsi que les champs de température et de vitesse axiale. On a trouvé des écoulements secondaires relativement élevés pour des différences de température entre la paroi et le fluide aussi faibles que 0,03 °C. Pour $(GP)^{\frac{1}{4}}$ plus grand que 30, la théorie de la couche limite semble être une bonne approximation du champ de température. Il existe des gradients de températures élevés près de la paroi ; les isothermes dans le noyau sont horizontales et il y a une variation sensible de température dans la direction verticale. Bien que l'écoulement secondaire avait un grand effet sur le champ de température, il en avait peu sur la distribution de vitesse axiale telle qu'elle a été prédite pour un nombre de Prandtl élevé. La configuration d'écoulement secondaire montrait des vitesses vers le haut relativement élevées près de la paroi et dans le noyau des vitesses vers le bas faibles. Les épaisseurs des couches limites de vitesse et de température sont approximativement égales. Ces résultats sont en accord avec un traitement du problème basé sur un raisonnement dimensionnel, qui a été présenté dans un article précédent venant de ce laboratoire.

RECHNERISCHE UND EXPERIMENTELLE UNTERSUCHUNG DES EINFLUSSES DER SEKUNDÄRSTRÖMUNG AUF DAS TEMPERATURFELD UND DIE PRIMÄRSTRÖMUNG IN EINEM BEHEIZTEN WAAGERECHTEN ROHR

Zusammenfassung—Das vollständig entwickelt Temperaturfeld und das axiale Geschwindigkeitsprofil

einer Flüssigkeit wurden am Austritt eines langen zylindrischen Rohres, das elektrisch beheizt ist, bei einer Prandtl-Zahl von 80 gemessen.

Die beschreibenden partiellen Differentialgleichungen, für das Sekundär-Strömungsfeld werden mit einem Differenzenverfahren gelöst und liefern sowohl das Temperaturfeld als auch das axiale Geschwindigkeitsfeld. Verhältnismässig grosse Sekundärströmungen wurden bei Temperaturdifferenzen von 0,05 °F zwischen der Aussenwand und der Flüssigkeit gefunden. Für $(GP)^{\frac{1}{4}}$ grösser als 30 erhält man mit der Grenzschttheorie eine gute Näherung für das tatsächliche Temperaturfeld. Grosse Temperaturgradienten treten in der Nähe der Aussenwand auf; die Isothermen im Kern verlaufen horizontal. Zu vertikaler Richtung besteht ein bedeutender Temperaturunterschied. Obwohl die Sekundärströmung das Temperatuefled stark verändert hat sie wenig Einfluss auf die Verteilung der axialen Geschwindigkeit, wie es für eine grosse Prandtl-Zahl vorausgesagt wurde. Das Sekundärströmungsfeld zeigte relativ grosse nach oben gerichtete Geschwindigkeiten nahe der Rohrwand und kleinere abwärts gerichtete Geschwindigkeiten im Kern. Die Dicke der Geschwindigkeits- und der Temperaturgrenzschicht sind annähernd gleich

Diese Ergebnisse stimmen mit einer Behandlung des Problems überein, die sich auf eine Dimensionsbetrachtung stützt und in einer vorhergehenden Veröffentlichung des Laboratoriums gezeigt wurde.

ЧИСЛЕННЫЙ РАСЧЕТ И ЭКСПЕРИМЕНТАЛЬНОЕ ИССЛЕДОВАНИЕ ВЛИЯНИЯ ВТОРИЧНОГО ПОТОКА НА ТЕМПЕРАТУРНОЕ ПОЛЕ И ОСНОВНОЙ ПОТОК В ГОРИЗОНТАЛЬНОЙ НАГРЕВАЕМОЙ ТРУБКЕ

Аннотация—Измерзны полностью развитые профили температуры и аксиальной скорости на выходе из длинной горизонтальной трубы, нагреваемой электрическим током при значении числа Прандтля жидкости равном 80. Определяющие дифференциалъные уравнения в частных производных решаются методом конечных разностей для описания моделей вторичного течения, а также температурного поля и аксиальной скорости. Для разностей температуры стенки и жидкости в 0,05°F найдены относительно большие вторичные течения. Оказывается, что при $(GP)^{1/4} > 30$ температурное поле хорошо аппроксимируется с помощью теории пограничного слоя. У стенки имеют место большие температурные градиенты; изотермы в ядре являются горизонталными, и в вертикальном направлении происходит значительное изменение температуры. Хотя вторичное течение оказывает большое влияние на температурное поле, оно мало влияет на распределение аксиальной скорости, как было рассчитано для большого числа Прандтля. Вблизи стенок имеют место относительно большие направленные вверх скорости вторичных течений и малые направленные вниз скорости в ядре. Толщины пограничных слоев скорости и температуры приближенно равны. Эти результаты согдасуются с данными размерного анализа, представленного в предыдущей статье данной лаборатории.